Molecular Crystals and Liquid Crystals

Publication details, including instructions for authors and subscription information:
http://www.tandfonline.com/loi/gmcl20

Effect of Pressure on Phase Behavior of Thermotropic Cubic Mesogens 1,2-bis-(4-n-alkyloxybenzoyl)hydrazine

Yoji Maeda [a] , Takeya Ito [b] , Shoichi Kutsumizu [b] , Kazuya Saito [c] & Michio Sorai [d]

[a] Nanotechnology Research Institute, National Institute of Advanced Industrial Science and Technology, Higashi, Tsukuba, Ibaraki, Japan

[b] Department of Chemistry, Gifu University, Yanagido, Gifu, Japan

[c] Department of Chemistry, Graduate School of Pure and Applied Science, University of Tsukuba, Tennodai, Tsukuba, Ibaraki, Japan

[d] Research Center for Molecular Thermodynamics, Graduate School of Science, Osaka University, Toyonaka, Osaka, Japan

Version of record first published: 31 Aug 2006

To cite this article: Yoji Maeda, Takeya Ito, Shoichi Kutsumizu, Kazuya Saito & Michio Sorai (2005): Effect of Pressure on Phase Behavior of Thermotropic Cubic Mesogens 1,2-bis-(4-n-alkyloxybenzoyl)hydrazine, Molecular Crystals and Liquid Crystals, 436:1, 177/[1131]-201/[1155]

To link to this article: http://dx.doi.org/10.1080/15421400590956153

Mol. Cryst. Liq. Cryst., Vol. 436, pp. 177/[1131]–201/[1155], 2005

ISSN: 1542-1406 print/1563-5287 online
DOI: 10.1080/15421400590956153

Taylor & Francis
Taylor & Francis Group

Effect of Pressure on Phase Behavior of Thermotropic Cubic Mesogens 1,2-bis-(4-*n*-alkyloxybenzoyl)hydrazine

Yoji Maeda
Nanotechnology Research Institute, National Institute of Advanced Industrial Science and Technology, Higashi, Tsukuba, Ibaraki, Japan

Takeya Ito
Shoichi Kutsumizu
Department of Chemistry, Gifu University, Yanagido, Gifu, Japan

Kazuya Saito
Department of Chemistry, Graduate School of Pure and Applied Science, University of Tsukuba, Tennodai, Tsukuba, Ibaraki, Japan

Michio Sorai
Research Center for Molecular Thermodynamics, Graduate School of Science, Osaka University, Toyonaka, Osaka, Japan

Phase behavior of four homologues compounds of optically isotropic, thermotropic cubic mesogens 1,2-bis-(4-n-alkyloxybenzoyl)hydrazine, BABH(n), n indicating the number of carbon atoms in the alkyloxy chain, was investigated under pressures up to 300 MPa using a high-pressure differential thermal analyzer, a wide-angle X-ray diffractometer and a polarizing optical microscope equipped with a high-pressure optical cell. The transition sequence for BABH(8) and BABH(10), low-temperature crystal (Cr_2)–high-temperature crystal (Cr_1)–cubic (Cub)–smectic C (SmC)–isotropic liquid (I) observed under atmospheric pressure, is held in the low pressure region below about 30 MPa and 10 MPa, respectively. The triple points for the SmC, Cub and Cr_1 phases are estimated as 31.6 ± 2.0 MPa, 147.0 ± 1.0 °C and 11.0 ± 1.0 MPa, 144.0 ± 1.0 °C for BABH(8) and BABH(10), respectively, indicative of the upper limit of pressure for the formation of the cubic phase. The thermodynamic analysis using the Clausius–Clapeyron equation

S. K. is grateful for financial support from the Ministry of Education, Culture, Sports, Science, and Technology, Japan [Grant-in-Aid for Scientific Research No.413/13031037 and 14045232, and (C) 14550846]. K. S. and M. S. are grateful for financial support from the Ministry of Education, Culture, Sports, Science, and Technology, Japan [Grant-in-Aid for Scientific Research (A) (11304050)].

Address correspondence to Yoji Maeda, Nanotechnology Research Institute, National Institute of Advanced Industrial Science and Technology, Higashi 1-1, Tsukuba, Ibaraki 305-8565, Japan. E-mail: yoji.maeda@aist.go.jp

suggests strongly that the Cub–SmC transition with negative slope (dT/dP) accompanies with negative volume of transition. BABH(11) and BABH(12) show the Cr_2–intermediate-temperature crystal (Cr_3)–Cr_1–Cub–I transition sequence at pressures below 10–12 and 16–17 MPa, respectively. When higher pressure is applied, the SmC phase with schlieren texture is induced between the isotropic liquid and cubic phases. A biphasic sea-island texture consisting of the SmC and the cubic phases can be seen on heating in the wide pressure region up to 140 MPa. These observations exhibit the destabilization of the cubic phase with increasing pressure.

Keywords: Cub–SmC transition; high-pressure DTA; *in-situ* POM observation; pressure-induced SmC phase; thermotropic cubic mesogen; *T–P* phase diagram; triple point

1. INTRODUCTION

Since Gray *et al*. [1] reported in 1957 the synthesis of 4′-*n*-hexadecyloxy- and 4′-*n*-octadecyloxy-3′-nitrobiphenyl-4-carboxylic acid: referred to as ANBC(16) and ANBC(18), respectively, a number of thermotropic cubic mesogens have been studied [2]. The majority of these compounds are carbohydrates and polycatenar compounds including several examples of metallomesogens. 1,2-bis-(4-*n*-alkyloxybenzoyl) hydrazine, denoted as BABH(*n*), where *n* indicates the number of carbon atoms in the alkoxy chain, were synthesized by Schubert *et al*. [3] and it belongs to the classical thermotropic cubic mesogens. The chemical structure of 1,2-bis-(4-*n*-alkyloxybenzoyl)hydrazine BABH(*n*) is shown below.

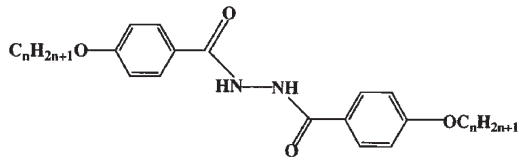

n = 8, 10, 11, 12

As reported by Demus *et al*. [4], the octyloxy-, nonyloxy- and decyloxy-homologues of the BABH(*n*) series exhibit both cubic (Cub) and smectic C (SmC) phases, and show the phase sequence of low-temperature crystal (Cr_2)–high-temperature crystal (Cr_1)–Cub–SmC–isotropic liquid (I). Göring *et al*. [5] determined the crystal structure of BABH(8) as well as the structures of the cubic and SmC phases. The BABH(8) molecules in the crystalline phase form sheets linked by hydrogen bonds. The precise calorimetric measurements on BABH(8) were carried out by Sorai and his collaborators [6], and provided the reliable thermodynamic quantities of the phase transitions.

In lyotropic systems the general accepted explanation of the cubic structure with the space group *Ia3d* is the jointed-rod model [7,8], where rod micelles are linked three-by- three to form two networks which are interwoven but not connected [2,7–13]. An alternative representation is based upon the interface between the hydrophilic part of the amphiphilic molecules and the water molecules which build a bicontinuous infinite periodic minimal surface (IPMS) that divides the space into two parts [2,9,11–16]. The three simplest cubic IPMS are shown mathematically to be the Schöen Gyroid G (space group *Ia3d*), and the P and D Schwarz surfaces (space groups *Im3m* and *Pn3m*), respectively [14,15]. The space group *Ia3d* is related to the gyroid G in which the IPMS forms two interwoven labyrinths, each of which covers the three-by-three jointed rods. The diffracted intensity by a G surface decorated by layer was calculated and the theoretical predictions fit with the experimental data obtained for direct and inverted *Ia3d* cubic phases [17]. But its application for the thermotropic cubic phases needs an explanation of the formation of rods by the molecules of the pure compounds. Recently a quasi-binary (QB) picture [18,19] for the thermotropic cubic systems is proposed on the basis of thermodynamic observations [6, 20–27]. The experimental conformational entropy of long alkyl chains attached to the rigid core of mesogenic molecules indicates that the alkyl chains are highly disordered in the liquid crystalline states. The disordered alkyl chains are regarded as 'intramolecular solvent' or 'self-solvent' judging from a close resemblance between phase diagrams of neat and binary systems. The QB picture is shown to be applicable to the examples of classical thermotropic cubic phases: the essential structural motif is TPMS (or IPMS) surface.

The authors studied the phase behavior of the ANBC(n) homologous series under hydrostatic pressure using a high-pressure differential thermal analyzer (DTA). They reported an interesting T *vs.* P phase diagram of ANBC(16) in the heating and cooling modes [28,29]: there is a triple point for the SmC, Cub and SmA phases at about 54 MPa and 205°C, indicative of the upper limit of pressure for the formation of the cubic phase. A columnar phase appears reversibly in the place of the cubic phase under elevated pressures above 60–80 MPa, showing the $I \leftrightarrow SmA \leftrightarrow Col \leftrightarrow SmC \leftrightarrow Cr$ transition sequence. But the columnar phase appears monotropically in the low pressure region including atmospheric pressure, exhibiting the phase sequence of $I \leftrightarrow SmA \rightarrow Col \rightarrow Cub \leftrightarrow SmC \leftrightarrow Cr$ [30]. As is already reported by Demus *et al*. [4], BABH(n) with n ranging from $n = 8$ to $n = 10$ show the $Cr_2 \leftrightarrow Cr_1 \leftrightarrow Cub \leftrightarrow SmC \leftrightarrow I$ phase transition sequence under atmospheric pressure. In these compounds the cubic phase is located

on the low temperature side of the SmC phase, while the cubic phase of ANBC(n) appears on the high temperature side. The inversion in phase sequence of BABH(n) compounds prompted us to investigate the phase behavior of the BABH(n) homologous series under hydrostatic pressure, with particular focus on the effect of pressure on the phase stability of the cubic phase.

In this paper, we present the experimental results of the thermal, morphological and structural behavior of the four BABH(n) homologous compounds with $n = 8$, 10, 11 and 12 under hydrostatic pressures up to 300 MPa using a high-pressure DTA, a polarizing optical microscope (POM) equipped with a high-pressure optical cell, and a wide-angle X-ray diffractometer (WAXD) equipped with a high-pressure vessel.

2. EXPERIMENTAL

2.1. Sample Characterization under Ambient Pressure

BABH(8) and BABH(10) samples used in this study were prepared as described in [3]. BABH(11) and BABH(12) samples also were synthesized similarly. The samples had been recrystallized from ethanol several times and the purity was confirmed by infrared (IR), ^{1}H NMR, mass spectroscopy, and elemental analysis. Thermal characterization of the samples was performed on a Perkin-Elmer DSC-7 and Seiko Instruments SSC-5000 differential scanning calorimeters at a scanning rate of 5°C min^{-1} under N_2 gas flow. Temperatures and heats of transition were calibrated using the standard materials (indium and tin). Transition temperatures were determined as the onset of the transition peaks at which the tangential line of the inflection point of the rising part of the peak crosses over the extrapolated baseline. Morphological characterization was performed using a Leiz Orthoplan POM equipped with a Mettler hot stage FP-82.

2.2. DTA Measurements under Pressure

The high-pressure DTA apparatus used in this study is described elsewhere [32]. The DTA system was operated in a temperature region between room temperature and 250°C under hydrostatic pressures up to 200 MPa. Dimethylsilicone oil with a medium viscosity (100 cSt) was used as the pressurizing medium. The sample weighing about 4 mg was put in the sample cell and coated with epoxy adhesives, to fix the sample in the bottom of the cell and also to prevent

direct contact with the silicone oil. The DTA runs were performed at a constant scanning rate of $5^{\circ}C\,min^{-1}$ under various pressures. Peak temperatures were adopted as transition temperatures for making the real temperature vs. pressure phase diagram.

2.3. Morphological and X-ray Characterization under Pressure

The optical texture observation of the samples under hydrostatic pressure was performed using a Leitz Orthoplan POM equipped with a high-pressure optical cell system [33]. Transmitted light intensity through the POM with crossed Nicols was measured using a Mettler FP-90 photomonitor under atmospheric and hydrostatic pressures. The texture observation was performed both on heating and cooling processes under isobaric conditions and during the pressure change in isothermal conditions in the pressure range up to 150 MPa.

Structural changes during the phase transition under pressure were observed using a high-pressure WAXD apparatus [32]. The high-pressure vessel was set on the wide angle goniometer of a 12 kW rotating anode X-ray generator (Rotaflex RU200, Rigaku Co.). The sample was inserted into the vertical hole of the beryllium spindle as the pressure cell. The beryllium spindle was mechanically compressed for pressure sealing using the upper and lower pressure blocks. Then the sample was pressurized hydrostatically at pressures up to 300 MPa. A Ni-filtered Cu Kα X-ray was used to irradiate the sample, and the diffraction patterns were obtained using an imaging plate detector (BAS-IP 127×127 mm, Fuji Photo Film Co.).

3. EXPERIMENTAL RESULTS

The plot of the transition points of the BABH(n) homologues series as a function of the number of carbon atoms in the alkoxy chain is shown in Figure 1. As reported by Demus *et al*. [4], the octyloxy- ($n = 8$), nonyloxy- ($n = 9$) and decyloxy- ($n = 10$) homologues exhibit both Cub and SmC phases, and show reversibly the phase sequence Cr_2–Cr_1–Cub–SmC–I. Sorai and his collaborators [6] reported the precise transition points on BABH(8), close to the Demus *et al*.'s data. Kutsumizu *et al*. [31] reported that the undecyloxy- ($n = 11$), dodecyloxy- ($n = 12$) and tetradecyloxy- ($n = 14$) homologues show only the cubic phase between the crystal and isotropic liquid, indicative of the phase sequence of Cr_2—intermediate-temperature crystal (Cr_3)–Cr_1–Cub–I under atmospheric pressure.

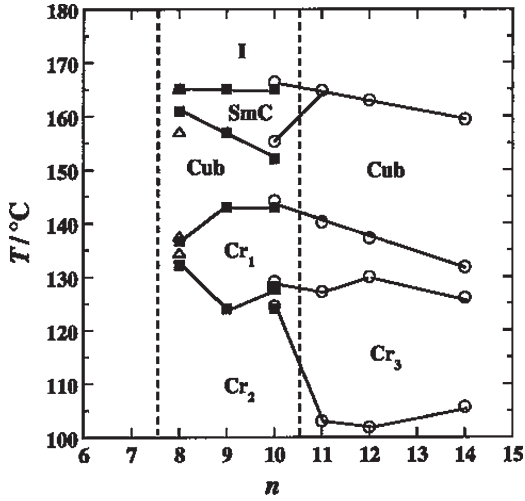

FIGURE 1 Transition points of the BABH(n) homologues series as a fuction of the number of carbon atoms n in the alkoxy chain. Data points from the Demus *et al*., Sorai *et al.*, and Kutsumizu *et al*. are shown by the symbols ■, △, and ○, respectively.

3.1. Babh(8) and Babh(10)

BABH(8) and BABH(10) show reversibly the $Cr_2 \leftrightarrow Cr_1 \leftrightarrow Cub \leftrightarrow SmC \leftrightarrow I$ transition sequence under atmospheric pressure [3–6]. The cubic phase is held in a temperature range of about 20°C. Figure 2 shows the POM photographs of the typical textures of BABH(10) on heating under atmospheric pressure. When the crystal melts at about 140°C, a completely black field of view for the cubic phase is seen. Then a sea-island texture of bright islands in the dark sea appears, Figure 2c, indicating the gradual growth of the SmC phase in the predominant cubic phase. The co-existing sea-island texture at 161°C, Figure 2d, exhibits the slow transition from the cubic to the SmC phases. The schlieren texture of the SmC phase is grown in the whole field of view at 165°C, Figure 2e, and then disappears into the dark field of view for the isotropic liquid at 166°C. The same change in texture for BABH(8) is observed under atmospheric pressure.

The morphological observation of BABH(8) and BABH(10) was performed under both isobaric and isothermal conditions [34,35]. The isobaric observation of BABH(10) at 5 MPa exhibits the same morphological change as those observed at atmospheric pressure in Figure 2. Figure 3 shows the change in texture of BABH(10) on

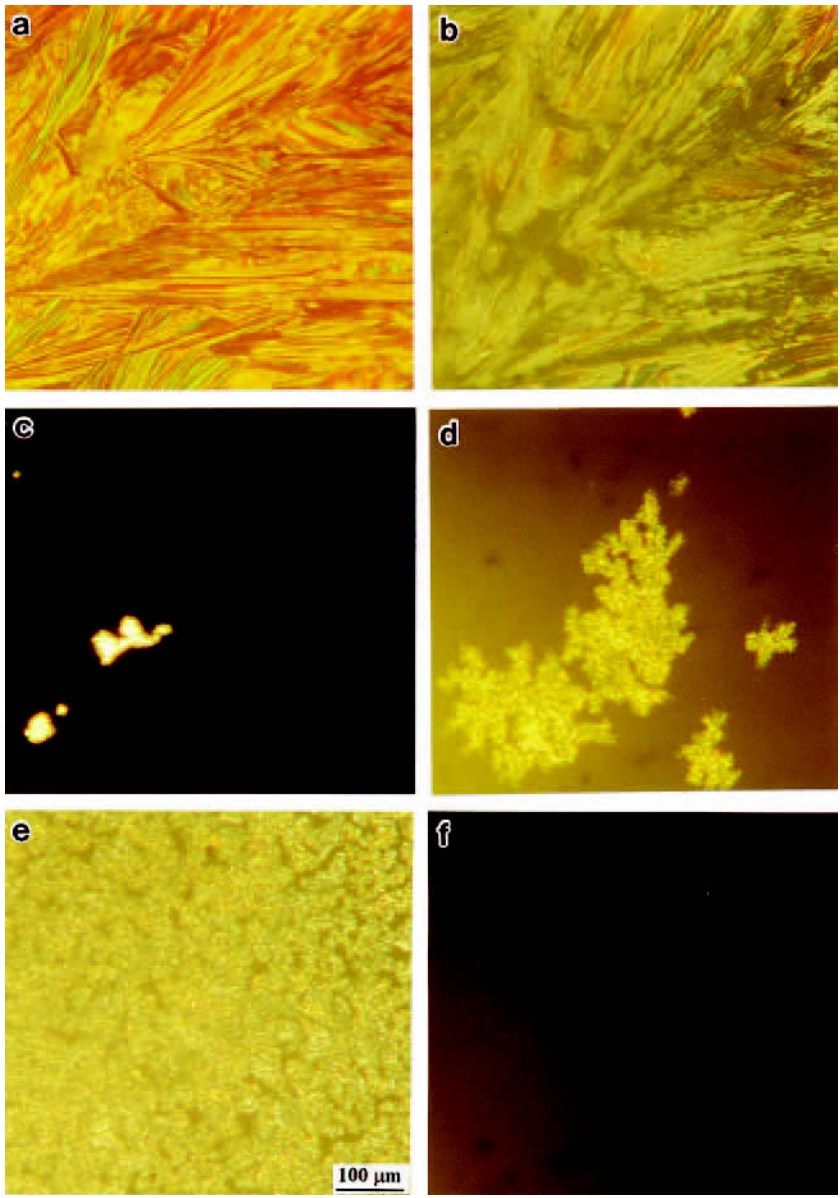

FIGURE 2 POM micrographs of BABH(10) on heating at atmospheric pressure: (a) Cr_2 at 25°C; (b) Cr_1 at 135°C; (c) Cub at 144°C; (d) Cub → SmC transition at 161°C; (e) SmC at 165°C; (f) isotropic liquid at 166°C. (from [35], reproduced by permission of Taylor & Francis, Ltd.)

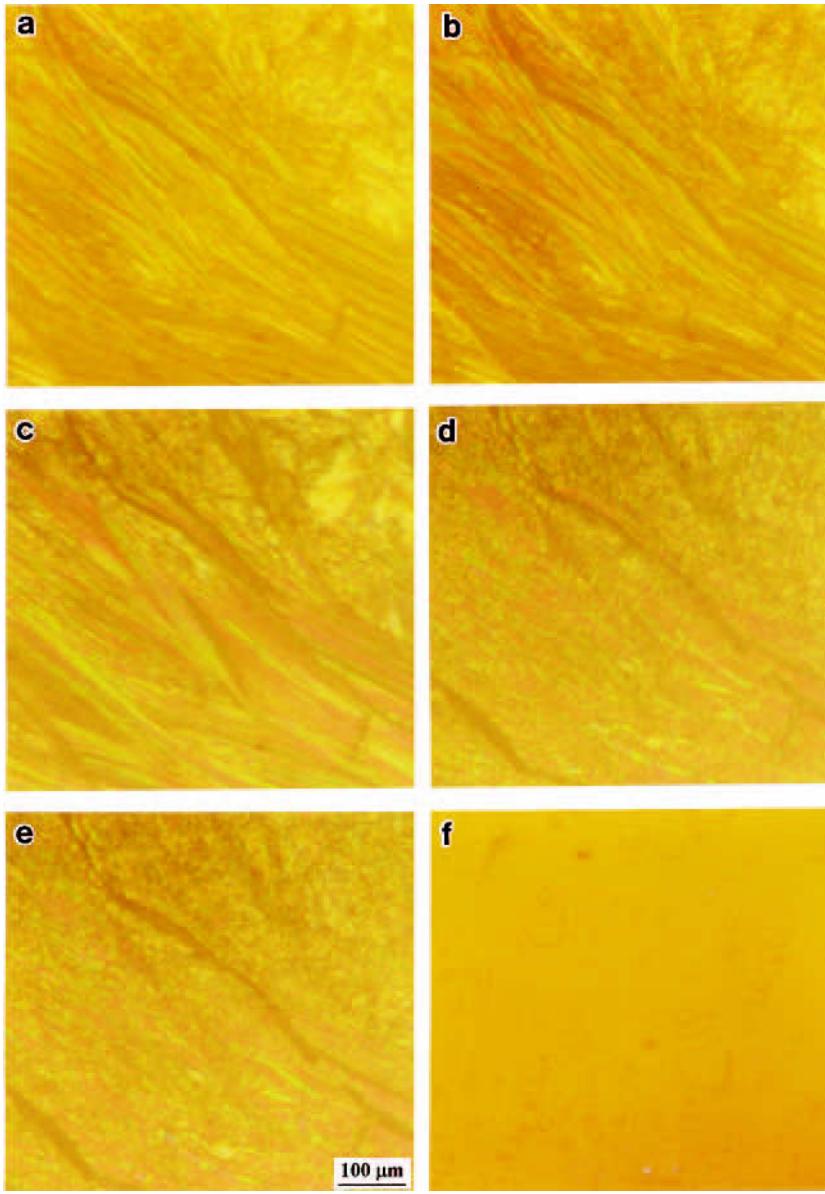

FIGURE 3 POM micrographs of BABH(10) on heating at 10 MPa.: (a) Cr_2 at 25°C; (b) Cr_3 at 115°C; (c) Cr_1 at 138°C; (d,e) SmC at 145 and 160°C; (f) isotropic liquid at 170°C. (from [35], reproduced by permission of Taylor & Francis, Ltd.)

heating at 10 MPa. The crystalline texture changes directly into the schlieren texture of the SmC phase, Figures 3d and 3e, and the texture is held until the isotropization occurs at 167°C. It is noted that the cubic phase does not appear during the runs at 10 MPa and higher pressures [35]. One can see that the Cr_2–SmC–I transition sequence is observed at high pressures above about 30 MPa for BABH(8) and at 10–12 MPa for BABH(10), respectively [34,35]. The isothermal observation of the texture of the cubic phase was performed to investigate the effect of pressure on the stability of the cubic phase. Figure 4 shows the POM photographs of the cubic phase of BABH(10) in an isothermal path at 152°C. When pressure is raised from 2 to 5 MPa, the yellowish, not black, field of view for the cubic phase, Figure 4a, changes to the schlieren texture, Figures 4b and 4c, indicating the occurrence of the Cub–SmC transition in the isothermal process. When the pressure is released, many black spots of the cubic phase are sporadically formed in the schlieren texture of the SmC phase by annealing for 30 min at 152°C and 1 MPa, Figure 4e, and such black-spot pattern of the sea-island texture is held even at 0.1 MPa, Figure 4f, indicating the incomplete recovery from the SmC phase to the cubic. It would take a long period of time for the completion of the SmC → Cub transition by pressure releasing at 152°C. The sea-island texture changes completely to the yellowish featureless texture of the cubic phase by decreasing temperature to 145°C. The isothermal experiments also exhibit the reversible Cub–SmC transition like the transition on heating and cooling under atmospheric pressure. The same morphological behavior was observed at 145°C in an isothermal path. The different transition pressures observed at 152 and 145°C lead to a negative slope (dT/dP) of the Cub–SmC transition line in the phase diagram [34,35]. The relation of the Cub–SmC transition points to pressure for BABH(10) is obtained from the *in-situ* morphological observations at various pressures: the Cub–SmC transition line with a negative slope (dT/dP) crosses with the Cr_1–Cub line with a positive slope at about 10–12 MPa. [35].

Figure 5 shows the X-ray diffraction patterns of the cubic phase of BABH(8) at 135°C and 1 MPa, the SmC phase at 165°C and 25 MPa, and the SmC phase at 181°C and 100 MPa, respectively [34]. The spot pattern for the cubic phase, Figure 5a, is closely resembled with that of the cubic phase of an oriented sample by Göring *et al*, who reported the reliable results on monodomain sample [5]. Several low-angle peaks for the cubic phase are due to the reflections from the {211} plane at $2\theta = 3.18^\circ$ ($d = 2.77$ nm) and {220} reflections. The {001} reflection of the SmC phase at 165°C and 25 MPa, Figure 5b, is observed at $2\theta \cong 3.5^\circ$ ($d = 2.54$ nm). The X-ray pattern of the SmC phase

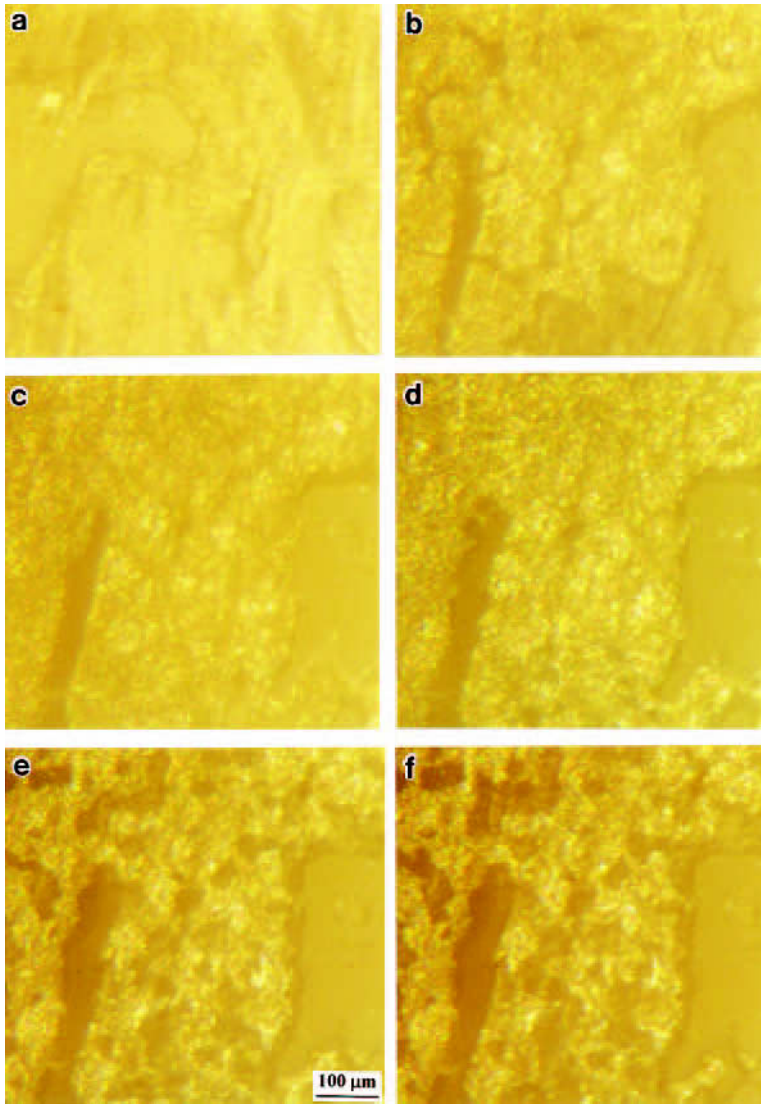

FIGURE 4 POM photographs of the change in texture of the cubic phase of BABH(10) in a isothermal path at 152°C: (a) Cub at 2 MPa; (b,c) sea-island texture of bright sea with schlieren texture (SmC) and dark island (Cub) at 3 and 5 MPa in the pressurizing process; (d) the same texture as (b,c) at 1 MPa in the subsequent pressure-releasing process; (e) gradual growth of the black spots (Cub phase) in the schlieren texture (SmC phase) after 30 min from (d); (f) more growth of the black spots (Cub phase) in the schlieren texture (SmC phase) at 0.1 MPa in the pressure-releasing process, exhibiting the incomplete transition of the SmC → Cub transition.

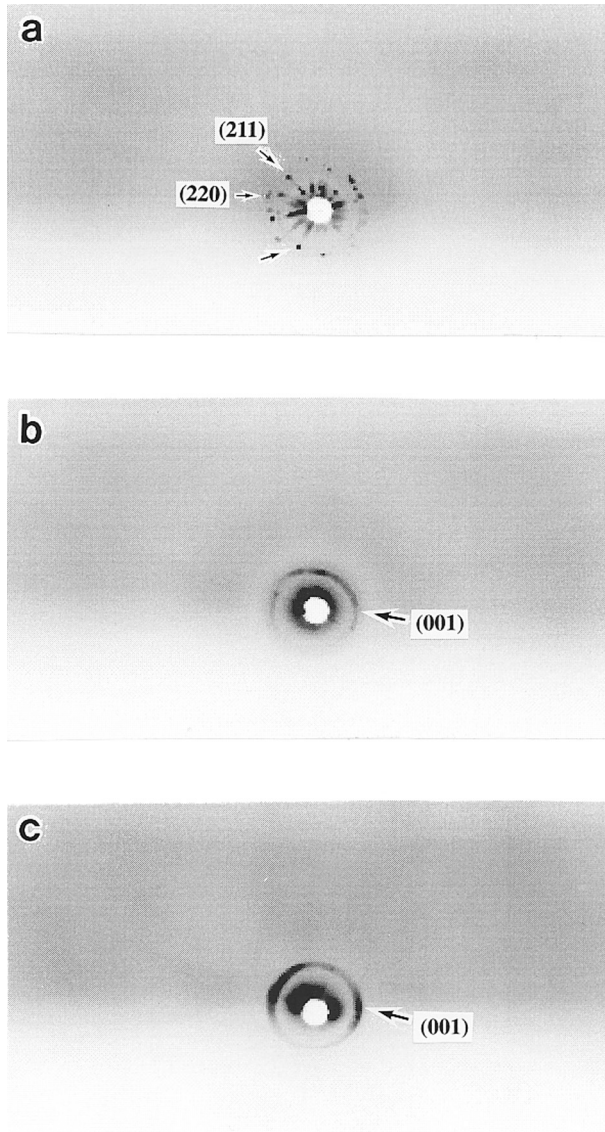

FIGURE 5 X-ray diffraction patterns of BABH(8): (a) cubic phase at 181°C and 1 MPa; (b) SmC phase at 165°C and 25 MPa; (c) SmC phase at 181°C and 100 MPa. (from [34], reproduced by permission of Taylor & Francis, Ltd.)

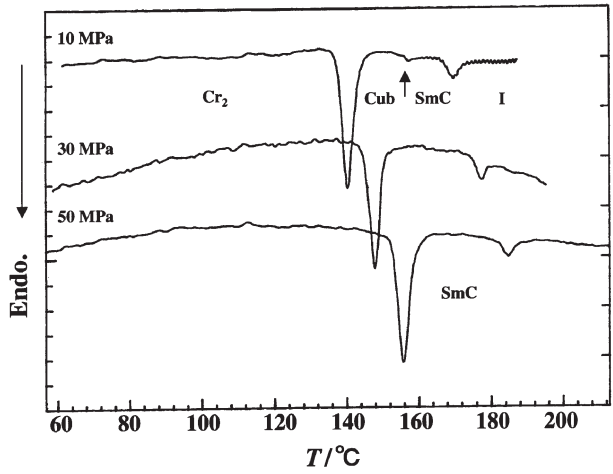

FIGURE 6 DTA heating curves of BABH(8) at 10, 30, and 50 MPa. (from [34], reproduced by permission of Taylor & Francis, Ltd.).

at 100 MPa, Figure 5c, is the same as that of the SmC phase at 25 MPa. The cubic phase is not observed under elevated pressures.

The thermal behavior of BABH(8) and BABH(10) was investigated under hydrostatic pressure. Figure 6 shows the DTA heating curves of BABH(8) at 10, 30, and 50 MPa. All the three curves show clearly a main peak due to the melting of the crystal and a small peak due to the SmC–I transition at high temperatures [34]. Only at 10 MPa another peak of the Cub → SmC transition is observed at an intermediate temperature, but it is not observed at higher pressures. In the case of BABH(10) the transition enthalpy of the Cub–SmC transition is barely observed on the DSC curve. Unfortunately the high-pressure DTA also is not useful for the Cub–SmC transition because the shortage of sensitivity and S/N ratio of the high-pressure DTA apparatus is clear for the measurements of such transitions with subtle heats of transition [35]. All the DTA heating curves of BABH(10) show two or three peaks corresponding to the melting and isotropization. Figure 7 shows the *T-P* phase diagrams of BABH(8) and BABH(10) under pressures up to 300 MPa. In BABH(8) and BABH(10) the Cub → SmC transition lines have its negative slopes (dT/dP) in the *T vs. P* phase diagrams, while the $Cr_1 \rightarrow$ Cub transition lines have normally positive slopes. So one can see that the cubic phase exists only in a small *T—P* region and does not appear at intermediate and high pressures. The triple points for the Cr_1, Cub

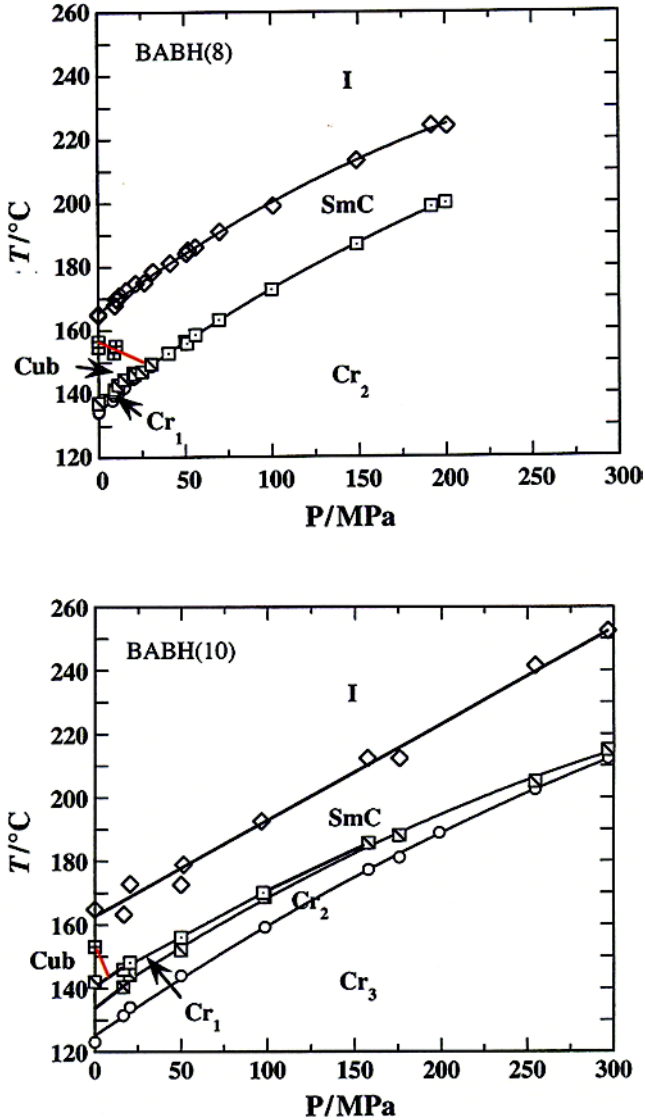

FIGURE 7 *T vs. P* phase diagrams of BABH(8) and BABH(10). (from [34,35], reproduced by permission of Taylor & Francis, Ltd.)

and SmC phases are estimated approximately as 31.6 ± 1.0 MPa, 147.0 ± 1.0°C for BABH(8) and 11.0 ± 1.0 MPa, 144.0 ± 1.0°C for BABH(10), respectively [34,35].

3.2. BABH(11) and BABH(12)

BABH(11) and BABH(12) exhibit the Cr_2–Cr_3–Cr_1–Cub–I transition sequence under atmospheric pressure [31]. They show only the morphological change between the crystalline spherulites and the black field of view for the cubic phase and also the isotropic liquid. The *in-situ* observations of the textures of BABH(11) and BABH(12) were performed both on isobaric and isothermal paths under pressure, to examine whether the cubic phase is stable under pressure [36]. Figure 8 shows the POM photographs of the textures of BABH(12) in the heating mode at 15 MPa. The spherulitic texture of the crystals is held at temperatures up to about 137–138°C. When temperature goes up beyond the Cr–Cub transition, the spherulitic texture vanishes and a ripple-like pattern as shown in Figures 8c and 8d appears in the cubic phase. The ripple- or mesh-like texture of the cubic phase is held just before the isotropization. These ripples or meshes may reflect the boundaries of the polydomains formed in the cubic phase. When temperature reaches to the isotropization point, the ripple- or mesh-like pattern is broken into small parts, as shown in Figure 8e, and disappears completely to the yellowish featureless fields of view for the isotropic liquid at 160°C, Figure 8f.

An increase of pressure induces an entirely different morphological texture for BABH(11) and BABH(12). Figure 9 shows the POM textures of BABH(12) in the heating mode at 30 MPa. The spherulitic texture of the crystals is held at temperatures up to about 140°C. A strange texture, Figure 9c, is observed at temperatures just above the melting point, which several black spots are born randomly in the bright spherulitic texture, indicating the Cr → Cub transition. When temperature goes up to higher temperature, the strange pattern changes to the typical sea-island texture, Figure 9d, in which the sea and island regions are assigned to the SmC and cubic phases, respectively. The sea-island texture consisting of bright sea (SmC phase) and dark islands (Cub phase) is held at temperatures up to the isotropization point. Furthermore one can see clearly that the isotropization starts around the dark islands and then the dark area of the isotropic liquid grows rapidly by consuming the schlieren texture of the sea region at 164°C, Figure 9e. So the bright sea region of the SmC phase decreases rapidly to the islands, Figure 9f, and then disappears to the brownish featureless field of view for the isotropic liquid at 167°C. When the sample is cooled from the isotropic liquid at 17 MPa and higher pressures, many small spheres with schlieren texture are generated in the dark field of view of the isotropic liquid [36], showing the formation of the pressure-induced SmC phase. The bright spheres

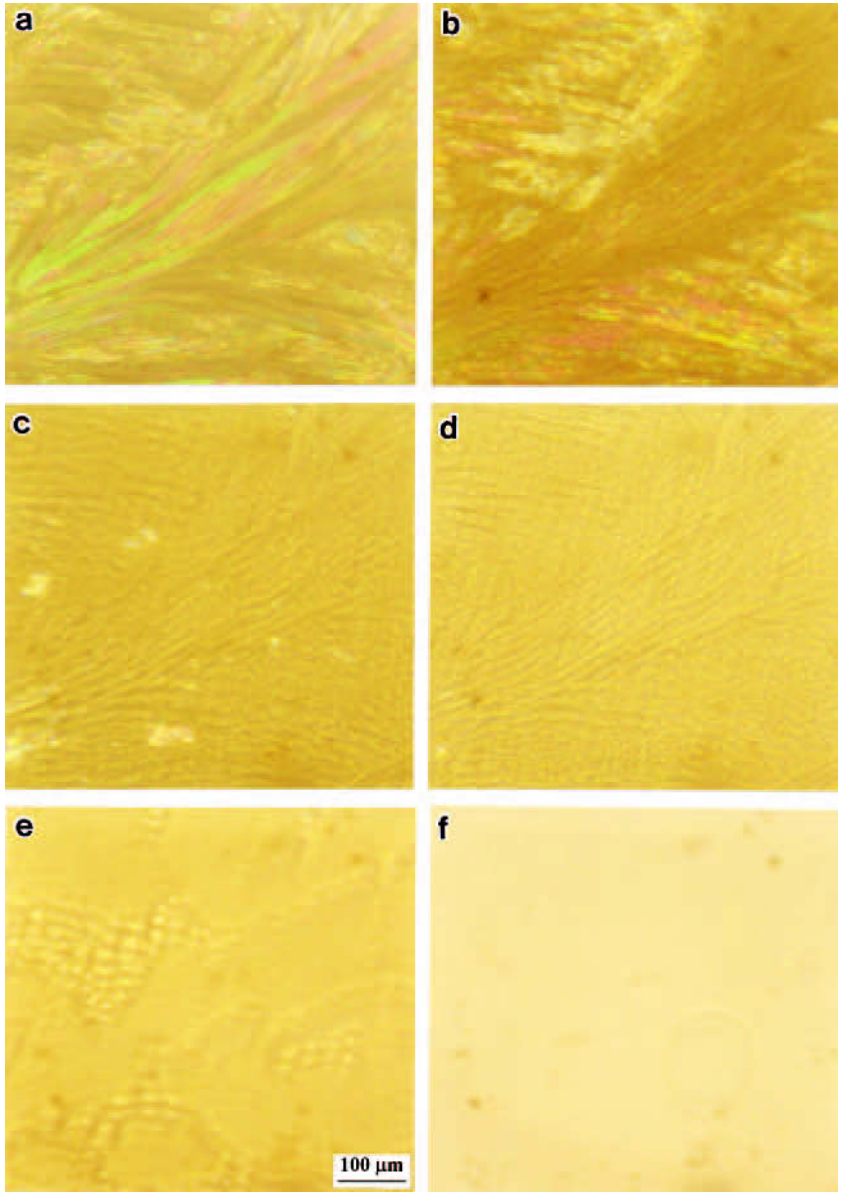

FIGURE 8 POM photographs of the textures of BABH(12) on heating at 15 MPa: (a) Cr_2 at 30°C; (b) Cr_1 at 138°C; (c,d) Cub phase at 139 and 150°C; (e) Cub → I transition at 159°C; (f) isotropic liquid at 160°C. (from [36], reproduced by permission of Taylor & Francis, Ltd.)

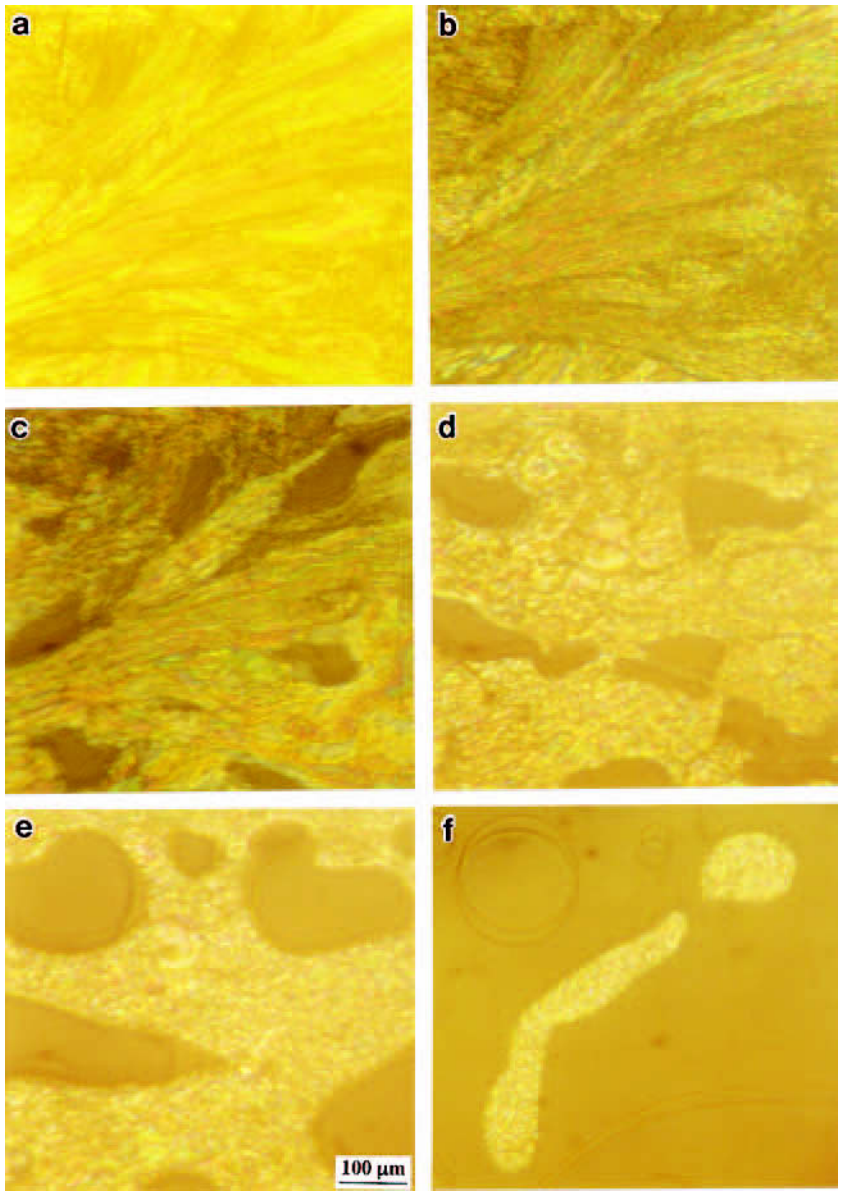

FIGURE 9 POM photographs of BABH(12) on heating at 30 MPa: (a) Cr_2 at 30°C; (b) Cr_1 at 140°C; (c,d) sea-island texture of the bright sea (SmC) and dark islands (Cub) at 141 and 157°C; (e) sea-island texture of the SmC and Cub phases at 164°C. One can see that isotropization starts around the cubic islands; (f) SmC → I transition at 166°C.

with schlieren texture grow with decreasing temperature, and they coalesce with each other to form the large schlieren texture of the SmC phase. The texture is observed at lower temperatures near the crystallization point. Then the SmC–Cub transition occurs rapidly and then followed by the crystallization. The morphological change of the texture of BABH(12) at 30 MPa indicates the reversible transition sequence of I–SmC–Cub–Cr, which is the same sequence as those of BABH(8) and BABH(10) observed under atmospheric pressure. Also in BABH(11) the pressure-induced SmC phase is observed at hydrostatic pressures above 10–11 MPa [36]. The bright sea–dark island texture of BABH(11) and BABH(12), indicative of the co-existence of the SmC and cubic phases, is similar to those observed in BABH(8) and BABH(10), but it is entirely reversed in composition: the dark sea (cubic phase)—bright island (SmC phase) texture in BABH(8) and BABH(10). Since the sea regions are predominant, the pressure-induced SmC phase for BABH(11) and BABH(12) is thought to be superior in phase stability over the cubic phase at 30 MPa and higher pressures.

Figure 10 shows the pressure dependence of the texture of the cubic phase of BABH(11) at 140°C during the isothermal path. The mesh-like texture, Figures 10a and 10b, of the cubic phase is held under pressures up to 11 MPa. These meshes are not regular, showing the short and long axis of several micron and $\sim$10 micron, respectively. When pressure is raised at 12 MPa, the dark and large blurred textures are grown rapidly over the mesh-like texture, Figure 10c. After 5 min of the (c) observation at 12 MPa, the texture shows a typical schlieren texture, Figure 10d, indicating the formation of the pressure-induced SmC phase [36]. When the applied pressure is released slowly, the schlieren texture, Figure 10e, is held at 10 MPa but the texture changes completely back to the mesh-like texture of the cubic phase at 4 MPa, Figure 10f. The reversible change in texture between the Cub and pressure-induced SmC phases is recognized in the isothermal path for BABH(11). The same morphological change between the mesh-like and schlieren textures for BABH(12) is observed at about 16–17 MPa. From the *in-situ* morphological observations the pressure-induced SmC phase is confirmed between the isotropic liquid and the cubic phase under hydrostatic pressures of about 10–12 and 16–17 MPa in BABH(11) and BABH(12), respectively [36]. The pressure-induced SmC phase exists preferably at higher pressures, but at the same time the SmC phase is co-existent with the cubic phase on heating in the wide pressure region. The biphasic sea-island textures for BABH(11) and BABH(12) are observed under elevated pressures up to 140 MPa [36].

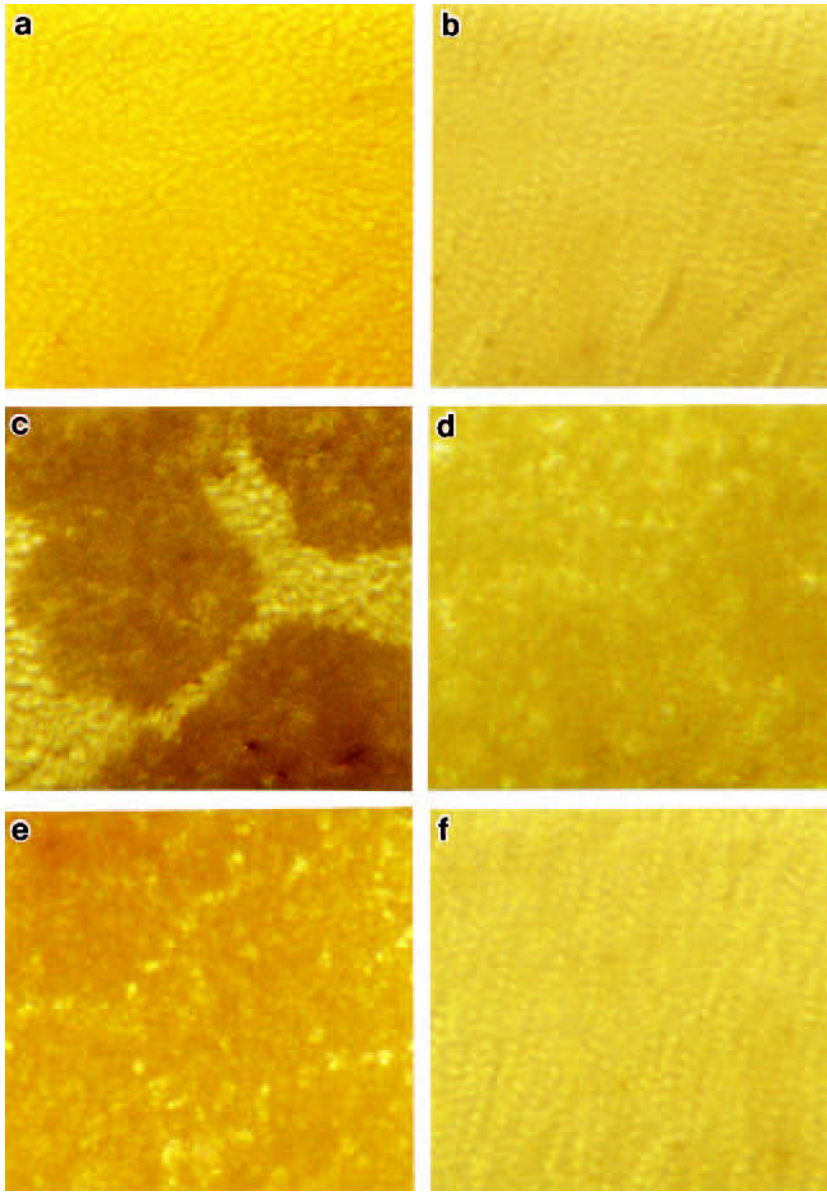

FIGURE 10 POM photographs of the change in texture of the cubic phase of BABH(11) at 140°C in the isothermal path: (a,b) mesh-like texture of the Cub phase at 3 and 10 MPa; (c) Cub → SmC transition at 12 MPa; (d) schlieren texture of the SmC phase at 12 MPa after 5 min; (e) schlieren texture of the SmC phase at 10 MPa in the pressure-releasing process; (f) mesh-like texture of the Cub phase at 4 MPa in the pressure-releasing process. (from [36], reproduced by permission of Taylor & Francis, Ltd.)

As is shown in Figure 5a for the cubic phase of BABH(8), the X-ray pattern of a nearly monodomain sample exhibits the spots located at each corner of a hexagon: they are assigned to {220} reflections and the other spots at each midpoint between the two neighboring vertices are assigned to {211} reflections, and thus the space group *Ia3d* is concluded. The same space group is confirmed for the cubic phase of BABH(11). In BABH(11) and BABH(12) the X-ray patterns under pressure correspond well to the POM textures observed at the same conditions. The spot-like X-ray pattern and the mesh-like texture for the cubic phase of BABH(12) at 150°C and 10 MPa changes to the Debye-Sherrer ring pattern and the schlieren texture for the SmC phase at 150°C and 30 MPa, respectively. The structural change between the cubic and SmC phases at 150°C occurs mainly in the pressure region between 15 and 20 MPa, corresponding to the morphological changes from the mesh-like to schlieren textures at 16–17 MPa. Two low-angle reflections of the cubic phase at 10 MPa are observed at $2\theta = 2.98^\circ$ ($d = 2.96$ nm) and $2\theta = 3.40^\circ$ ($d = 2.59$ nm), attributable to the (211) and (220) reflections of the *Ia3d* cubic lattice (a = 7.3 nm), respectively, while the (001) reflection of the SmC phase at 150°C is observed at $2\theta = 3.04^\circ$ ($d = 2.90$ nm).

The thermal behavior of BABH(11) and BABH(12) was investigated under pressure to study the phase stability of the cubic phase under pressure. The DTA heating curves show double peaks corresponding to the $Cr_2 \rightarrow (Cr_3\text{–}Cr_1)$ and $(Cr_3\text{–}Cr_1) \rightarrow$ mesophase transitions and a small peak for the mesophase →I transition at a higher temperature. The double peaks become close together with increasing pressure and merge to an apparently single peak at higher pressures above 200 MPa. This indicates the disappearance of the Cr_3 and Cr_1 phases at high pressures. The thermal behavior of BABH(12) under pressures is substantially the same as those in BABH(11). No mesophase transition in BABH(11) and BABH(12) was detected with the DTA measurements under pressures, but the formation of the pressure-induced SmC phase is apparent from the POM and X-ray observations, as described in the last paragraph. The *T* vs. *P* phase diagrams of BABH(11) and BABH(12) were constructed in the pressure region up to 300 MPa, based upon the thermal, morphological and structural experimental data. Figure 11 shows the *T*–*P* phase diagrams of BABH(11) and BABH(12). The boundary between the cubic phase and the pressure-induced SmC phase locates at about 10–12 MPa for BABH(11) and 16–17 MPa for BABH(12) [36]. The boundary lines shown by thick dotted lines in Figure 11 do not mean the phase transition lines as shown by red solid lines in Figure 7, but exhibits the lower limit of pressure for the formation of the SmC phase as a pressure-induced phase.

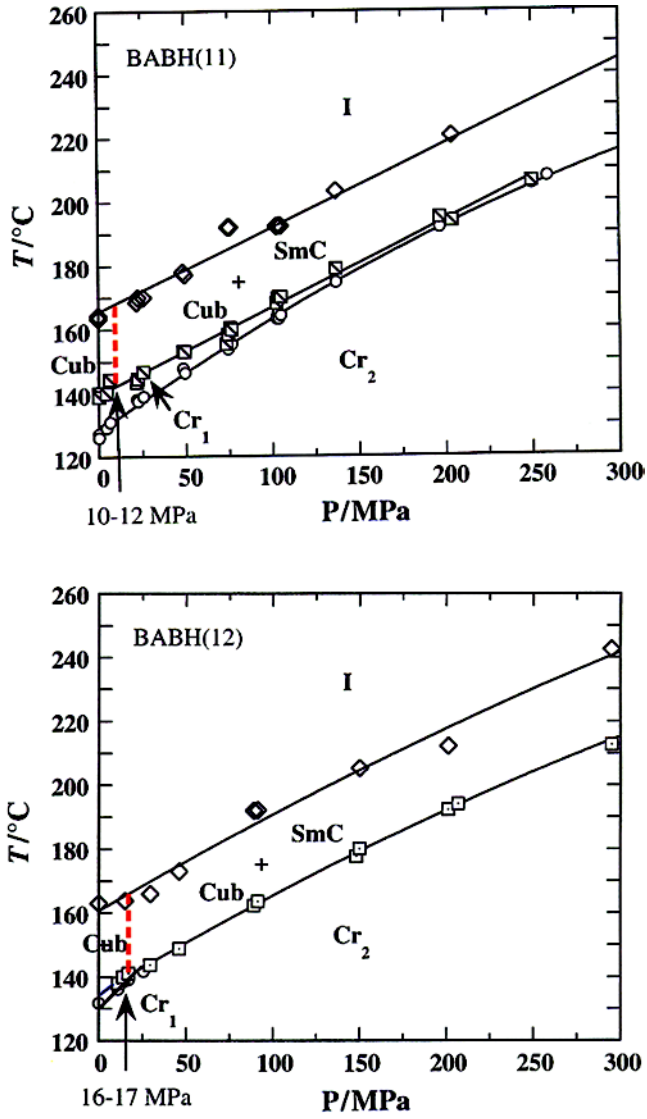

FIGURE 11 *T–P* phase diagrams of BABH(11) and BABH(12). Thick dotted lines do not show the phase transition lines, but only show the lower limit of pressure for the formation of the pressure-induced SmC phase. (from [36], reproduced by permission of Taylor & Francis, Ltd.)

4. DISCUSSION

The phase transition behavior of four BABH(n) homologous compounds with $n = 8$, 10, 11, and 12 was investigated under hydrostatic pressures up to 300 MPa. The temperature vs pressure phase diagrams of four samples were constructed. The disappearance of the cubic phase and the occupation of the SmC phase under pressure for BABH(8) and BABH(10), and the formation of the pressure-induced SmC phase for BABH(11) and BABH(12) are reasonably explained using the criteria of Gibbs energy-T relation in Figure 12. In BABH(8) and BABH(10), the Gibbs energy line of the cubic phase crosses over that of the SmC phase at a temperature between the melting and isotropization points under atmospheric pressure. When pressure is applied, the Gibbs energy line of the cubic phase moves substantially to higher levels, compared to those of other phases. The moving of the energy line to higher levels means the destabilization of the cubic phase with increasing pressure. Accordingly the Cub–SmC transition point lowers with increasing pressure, as shown in Figure 12 and the temperature region of the SmC phase broadens with pressure. At high pressures above the triple point the SmC phase exists stably between the crystal and the isotropic liquid phases. On the other hand, in BABH(11) and BABH(12) the Gibbs energy line of the cubic phase is always lower than that of the SmC phase at temperatures between the melting and isotropization points under atmospheric pressure. In this case the Gibbs energy line of the cubic phase would cross over that of the SmC phase at a temperature higher than the isotropization point. But the same story holds regarding the pressure effect of the cubic phase for BABH(11) and BABH(12), as illustrated in Figure 12.

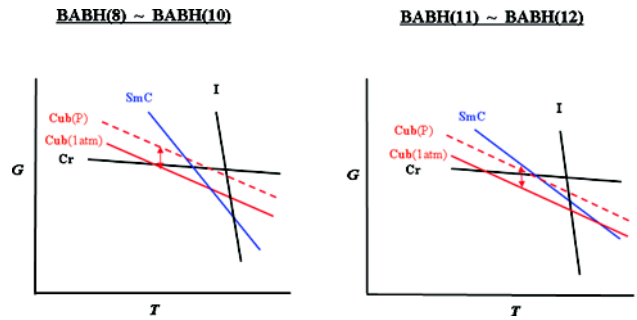

FIGURE 12 Schematic illustration of the phase transition behavior of BABH(n) using the criteria of Gibbs energy. (from [36], reproduced by permission of Taylor & Francis, Ltd.)

TABLE I Thermodynamic Quantities Associated with the Phase Transitions of BABH(8)

Phase transition	T°C	ΔH kJ mol^{-1}	ΔS JK^{-1} mol^{-1}	$(dT/dP)_{1atm}$	ΔV^* cm^3 mol^{-1}
Cr → Cub	133.5	51.8	127.4	0.420_1	53.5_2
Cub → SmC	153.7	1.34	3.1	-0.151_6	-0.4_7
SmC → I	163.4	7.17	16.4	0.464_1	7.6_1

*ΔV was deduced using the Clausius–Clapeyron equation.

The appearance of the pressure-induced SmC phase is explained reasonably using the hypothesis of the upper shift of the Gibbs energy line of the cubic phase with increasing pressure.

Application of the Clausius–Clapeyron equation to the Cub–SmC transition gives us another reasonable understanding of the existence of the SmC phase of BABH(8) and BABH(10) under pressures. Tables I and II list the thermodynamic quantities associated with the phase transitions of BABH(8) and BABH(10). From the thermodynamic data and the (dT/dP) data obtained using DSC and high-pressure DTA, the volume change of the transition is estimated using the equation $(dT/dP = \Delta V/\Delta S = T\Delta V/\Delta H)$. In BABH(8) and BABH(10) the Cub–SmC transition has the positive enthalpy of transitionΔH but shows the negative slope (dT/dP) of the transition line. So the volume change is assigned as negative, i.e., $\Delta V\ (\equiv V_{SmC} - V_{Cub}) < 0$. This expresses that the molar volume of the SmC phase is smaller than that of the cubic phase, i.e., the density of the SmC phase is higher than that of the cubic phase. That is why the SmC phase exists more stably than the cubic phase under pressure. The molecules in the SmC phase would be more densely packed than those in the cubic phase under pressure. Although in BABH(11) and BABH(12) (See Table III) the Cub–SmC transition lines are not determined at present, the same plausible

TABLE II Thermodynamic Quantities Associated with the Phase Transitions of BABH(10)

Phase transition	T°C	ΔH kJ mol^{-1}	ΔS JK^{-1} mol^{-1}	$(dT/dP)_{1atm}$	ΔV^* cm^3 mol^{-1}
$Cr_2 \rightarrow Cr_3$	122.0	24.3	61.5	0.371_9	22.9
$Cr_3 \rightarrow Cr_1$	127.1	4.9	12.2	0.357_4	4.4
$Cr_1 \rightarrow$ Cub	141.2	23.1	55.7	$.285_5$	15.9
Cub → SmC	153.0	0.4	0.9	-1.334_5	–1.2
SmC → I	163.9	7.2	16.4	0.305_0	5.0

*ΔV was deduced using the Clausius–Clapeyron equation.

TABLE III Thermodynamic Quantities Associated with the Phase Transitions of BABH(11) and BABH(12)

Phase transition	T°C	ΔH kJ mol^{-1}	ΔS JK^{-1} mol^{-1}	$(dT/dP)_{1atm}$	ΔV^* cm^3 mol^{-1}
BABH(11)					
$Cr_3 \rightarrow Cr_2$	51.4	3.3	10.2	—	—
$Cr_2 \rightarrow Cr_1$	125.3	30.9	77.6	0.295_1	22.9
$Cr_1 \rightarrow Cub$	137.1	22.6	55.1	0.273_2	15.1
$Cub \rightarrow I$	162.3	7.4	17.0	0.263_4	4.5
BABH(12)					
$Cr_3 \rightarrow Cr_2$	ca. 100	—	—	—	—
$Cr_2 \rightarrow Cr_1$	128.1	33.9	84.5	0.401_9	34.0
$Cr_1 \rightarrow Cub$	134.6	24.8	60.9	0.246_1	15.0
$Cub \rightarrow I$	161.2	7.1	16.4	0.268_6	4.4

*ΔV was deduced using the Clausius–Clapeyron equation.

explanation may be applicable. The Cub–SmC transition under pressure is schematically illustrated in Figure 13. The *Ia3d* cubic phase can be exhibited by either jointed–rod model [7,8,10,13] or IPMS structure model [9,11,14–17]. On the Cub–SmC transition the molar volume of the SmC phase would be smaller than that of the cubic phase, i.e., $V_{SmC} < V_{Cub}$ [35,36]. The relation of $V_{SmC} < V_{Cub}$ should be proved experimentally for the Cub–SmC transition of BABH(n) compounds for further discussion. In the case of ANBC(16) having the inverse phase sequence, Cr–SmC–Cub–SmA–I [14,15], which is popular for

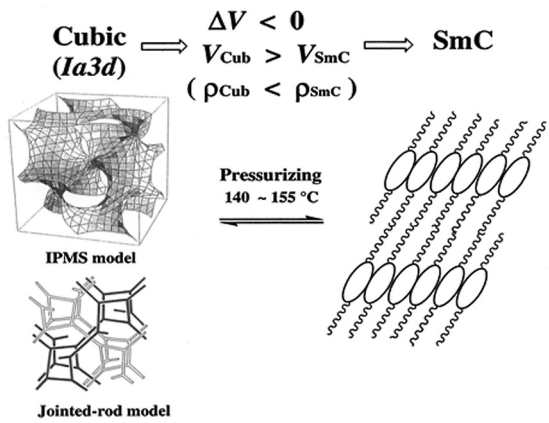

FIGURE 13 A plausible schematic illustration for the Cub–SmC transition of BABH(n) compounds in isothermal condition.

the typical thermotropic cubic mesogens, both the slope (dT/dP) and the transition enthalpy of the SmC → Cub transition are positive. Accordingly the relation of $\Delta V(\equiv V_{Cub}–V_{SmC}) > 0$ is held and thus the relation of $V_{SmC} < V_{Cub}$ holds for the SmC–Cub transition for ANBC(16) and its homologues. In reality the relation of $V_{SmC} < V_{Cub}$ is proved experimentally for ANBC(22) compound [37]. Thus the relation $V_{SmC} < V_{Cub}$ would be expected for the Cub–SmC transition of BABH(n) cubic mesogen. This suggests that the net volume of the cubic phase may be primarily determined not by the highly disordered alkyl chains but by the densely packed, three-dimensionally connected IPMS (infinitely periodic minimal surface) structure.

REFERENCES

[1] Gray, G. W., Jones, B., & Marson, F. (1957). *J. Chem. Soc.*, 393.
[2] Diele, S. & Göring, P. (1998). Chapter XIII. In: *Handbook of Liquid Crystals*, Demus, D., Goodby, J. W., Gray, G. W., Spiess, H.-W. & Vill, V. (Eds.), Wiley-VCH: Weinheim, Vol. 2B, 887–900.
[3] Schubert, H., Hauschild, J., Demus, D., & Hoffmann, S. (1978). *Z. Chem.*, *18*, 256.
[4] Demus, D., Gloza, A., Hartung, H., Hauser, A., Rapthel, I., & Wiegeleben, A. (1981). *Cryst. Res. Technol.*, *16*, 1445.
[5] Göring, P., Diele, S., Fischer, S., Wiegeleben, A., Pelzl, G., Stegemeyer, H., & Thyen, W. (1998). *Liq. Cryst.*, *25*, 467.
[6] Morimoto, N., Saito, K., Morita, Y., Nakasuji, K., & Sorai, M. (1999). *Liq. Cryst.*, *26*, 219.
[7] Luzzati, V. & Spegt, A. (1967). *Nature*, *215*, 701.
[8] Luzzati, V., Tardieu, A., Gulik-Krzywicki, T., Rivas, E., & Rerss-Husson, F. (1968). *Nature*, *220*, 485.
[9] Seddon, J. M. & Templer, R. H. (1993). *Phil. Trans. R. Soc. London*, *344*, 377.
[10] Tardieu, A. & Billard, J. (1976). *J. Phys. (Paris) Coll.*, *37*, C3-79.
[11] Charvolin, J. & Sadoc, J. F. (1990). *Colloid Polym. Sci.*, *268*, 190.
[12] Seddon, J. M., Hogan, J. L., Warrender, N. A., & Pebay-Peyroula, E. (1990). *Progr. Colloid Polym. Sci.*, *81*, 189.
[13] Levelut, A.-M. & Clerc, M. (1998). *Liq. Cryst.*, *24*, 105.
[14] Schwarz, H. A. (1890). *Gesammelte Math. Abhandlungen*, Bd. I., Springer: Berlin.
[15] Schön, A. H. (1969). *Not. Am. Math. Soc.*, *16*, 519.
[16] Hyde, S. T., Anderson, S., Ericsson, B., & Larson, K. (1984). *Z. Kristallogr.*, *168*, 213.
[17] Clerc, M. & Dubois-Violette, E. (1994). *J. Phys. II Fr.*, *4*, 275.
[18] Saito, K. & Sorai, M. (2002). *Chem. Phys. Lett.*, *366*, 56.
[19] Sorai, M. & Saito, K. (2003). *Chem. Rec.*, *3*, 29.
[20] Yamaguchi, T., Yamada, M., Kutsumizu, S., & Yano, S. (1995). *Chem. Phys. Lett.*, *240*, 105.
[21] Sato, A., Yamamura, Y., Saito, K., & Sorai, M. (1999). *Liq. Cryst.*, *26*, 1185.
[22] Saito, K., Sato, A., & Sorai, M. (1999). *Liq. Cryst.*, *25*, 525.
[23] Kutsumizu, S., Yamaguchi, T., Kato, R., & Yano, S. (1999). *Liq. Cryst.*, *26*, 567.
[24] Saito, K., Sato, A., Morimoto, N., Yamamura, Y., & Sorai, M. (2000). *Mol. Cryst. Liq. Cryst.*, *347*, 249.
[25] Saito, K., Shinhara, T., & Sorai, M. (2000). *Liq. Cryst.*, *27*, 1555.

[26] Saito, K., Shinhara, T., Nakamoto, T., Kutsumizu, S., Yano, S., & Sorai, M. (2002). *Phys. Rev. E*, *65*, 031719.
[27] Kutsumizu, S., Morita, K., Yano, S., & Nojima, S. (2002). *Liq. Cryst.*, *29*, 1459.
[28] Maeda, Y., Cheng, G.-P., Kutsumizu, S., & Yano, S. (2001). *Liq. Cryst.*, *28*, 1785.
[29] Maeda, Y., Prasad, S. K., Kutsumizu, S., & Yano, S. (2003). *Liq. Cryst.*, *30*, 7.
[30] Maeda, Y., Morita, K., & Kutsumizu, S. (2003). *Liq. Cryst.*, *30*, 157.
[31] Ito, T. & Kutsumizu, S. (2003). Bachelor thesis, Faculty of Engineering, Gifu University.
[32] Maeda,Y. & Kanetsuna, H. (1985). *Bull. Res. Inst. Polym. Tex.*, *149*, 119; Maeda, Y. (1990). *Thermochim. Acta.*, *163*, 211.
[33] Maeda, Y. & Koizumi, M. (1996). *Rev. Sci. Instrum.*, *67*, 2030; Maeda, Y. & Koizumi, M. (1998). *Rev. High Pressure Sci. Technol.*, *7*, 1532.
[34] Maeda, Y., Saito, K., & Sorai, M. (2003). *Liq. Cryst.*, *30*, 1139.
[35] Maeda, Y., Ito, T., & Kutsumizu, S. (2004). *Liq. Cryst.*, *31*, 623.
[36] Maeda, Y., Ito, T., & Kutsumizu, S. (2004). *Liq. Cryst.*, *31*, 807.
[37] Kutsumizu, S., Yamada, M., Tadano, K., Yano, S., Nojima, S., & Yamaguchi, T. (2004). *Mol. Cryst. Liq. Cryst.*, *412*, 49.